



# Development of High-Precision Ionospheric Monitoring System in China: Taking ROTI Map as an Example

Chengli She<sup>1,2(✉)</sup>, Haitao Liu<sup>3,4</sup>, Jun Yu<sup>2</sup>, Peiyuan Zhou<sup>2</sup>, and Hongzheng Cui<sup>2</sup>

<sup>1</sup> Qianxun Spatial Intelligence (Zhejiang) Inc., Deqing 313200, Zhejiang, China  
chengli.she@wz-inc.com

<sup>2</sup> Qianxun Spatial Intelligence Inc., Shanghai 200438, China

<sup>3</sup> State Key Laboratory of Lunar and Planetary Sciences, Macau University of Science and Technology, Macau 999078, China

<sup>4</sup> CNSA Macau Center for Space Exploration and Science, Macau 999078, China

**Abstract.** The ionosphere has always been one of the important error sources in GNSS navigation and positioning applications. The refined real-time monitoring of the ionosphere can provide more accurate information for calibration of ionospheric errors in high-precision positioning. Based on over 2,000 GNSS monitoring stations of the Beidou Ground-Based Augmentation System, this paper proposed a framework for the development of a high-precision ionospheric monitoring system in China, planning to provide a group of ionospheric products. Taking ROTI map as an example, the post-processing version has a spatial resolution of  $0.2^\circ$  in both longitude and latitude, with a temporal resolution of 30 s. The ROTI map with high-precision can not only indicate the area where the GNSS signal is severely affected by the ionosphere, but also provide an optimal strategy for satellite data selection in high-precision positioning applications.

**Keywords:** Ionosphere · Total electron content (TEC) · Rate of TEC index (ROTI) · Beidou Ground-Based Augmentation System (GBAS)

## 1 Introduction

In recent years, GNSS has been developing rapidly. The comprehensive completion of the Beidou Satellite Navigation and Positioning System (BDS) led by China has attracted widespread attention, and related applications are also accelerating by BDS. Nowadays, people have more and more precise requirements for positioning, timing, and navigation (PNT), where signals from navigation satellites are playing an increasingly important role in human production and life. The ionosphere acts as the only way for GNSS signals to propagate from upper satellites to the ground, whose impact on GNSS navigation and positioning is crucial.

For a long time, the ionosphere has always been a key factor affecting the accuracy of GNSS signal processing. Specifically, the ionospheric total electron content (TEC), as the line integral of the ionospheric electron density along the propagation path of

the GNSS signal, is generally used to measure the influence of the ionosphere upon the GNSS signal.

Constrained by the limitations of observation conditions, the ionospheric TEC is generally obtained by GNSS observations from fixed ground-based stations. Directly, the corresponding products are generated by ionospheric TEC observations, such as time series from single or multiple stations, and maps from local or global region. In addition, TEC derived parameters are also adopted as indicators for monitoring the ionosphere, for example, the rate of TEC index (ROTI).

As early as 1997, Pi et al. [1] analyzed the global distribution of ionospheric irregularities based on the scattering ROTI map calculated by global GPS observations. In particular, the ionosphere in Europe is plagued by auroral phenomena at night. Then, based on more than 700 GNSS stations located in the middle and high latitudes of the northern hemisphere, Cherniak et al. [2] develop regional ROTI map (geomagnetic latitude above 50°) under geomagnetic coordination, with bins of 2° along geomagnetic latitude and 8 min along geomagnetic local time, to specifically locate the active position of ionosphere in European area in research and applications.

However, the situation for China is quite different from Europe, since both the northern and southern regions of China have always been affected by the ionosphere, only the area in mid-latitudes is relatively less affected. On the one hand, for the southern region, such as Guangdong, Guangxi, Hainan provinces, generally located in geomagnetic low latitudes, the ionospheric equatorial abnormalities during the daytime and irregularities at nighttime occurs. On the other hand, for the northern region, such as Heilongjiang, Jilin, and Xinjiang provinces, the ionosphere is easily disturbed by the expansion of the aurora egg which expanded from polar region to lower latitudes at night. These phenomena have caused various impacts on the GNSS positioning in China. Therefore, the development of a map product which can reveal the ionospheric state grid by grid, has very important value in applications especially in real-time scenarios.

In order to meet the demand for real-time products of ionospheric maps, we plan to develop a high-precision ionospheric monitoring system, based on more than two thousand Beidou Ground-Based Augmentation System (GBAS) monitoring stations which are constructed and operated independently by ourselves. The planning products can provide rich information of ionosphere for real-time high-precision positioning. This paper will explain the architecture of this system, and take the development of ionospheric ROTI map during a major magnetic storm as an example.

## 2 High-Precision Ionospheric Real-Time Monitoring System in China

### 2.1 System Architecture

Based on the BDS GBAS stations, the architecture of the ionospheric monitoring system is shown in Fig. 1. The network, cloud, services and terminals constitute a complete closed-loop ecosystem. In this system, the network is the basis for the operation of the entire system which is composed of a number of densely distributed GBAS stations. The cloud, which relies on Alibaba cloud computing capabilities, is the core of the system

implementation, and is responsible for the real-time Collection, processing and output of data. Meanwhile, the service of ionospheric monitoring, acting as relatively independent service, reuses the data resources on the cloud to obtain a group of products in the form of maps. Finally, the ionospheric products can be delivered to users by network protocols such as NTRIP in real-time, sharing the real-time perception of the ionospheric status at both the server and terminals, in order to alleviate the impact of the ionosphere on positioning as much as possible.



**Fig. 1.** Architecture of ionospheric real-time monitoring system

## 2.2 Network-Cloud-Map-End Integrated Solutions

The network-cloud-end integrated solution is an emerging collaborative solution in the Internet era. The cloud platform organically combines massive data resources and out-of-conventional computing power. It provides a modular scheduling method suitable for loading various calculations and easy delivering to different users. Before, GNSS-based ionospheric monitoring solutions were mainly implemented by GPS monitoring stations. The average distance between these monitoring stations can reach more than 100 km or even longer. The equipment in those stations is slowing updated, and generally not support the G/R/C/E multi-GNSS signals. Therefore, the ability to finely detect the ionosphere is limited. At the same time, those solutions are usually only available for professional users, such as the military and scientific research institutes, instead of ordinary users. According to the solution proposed in this paper, ordinary users can also obtain real-time information of ionosphere like professional users, by this way various terminals can be adapted more flexibly. Meanwhile, the applications from different terminals can help improve and broaden the ionospheric monitoring services, to build a more diverse ecosystem.

## 2.3 High-Precision Ionospheric Map Service

The goal of the high-precision ionospheric map service is to provide grided real-time ionospheric map datasets in China, as shown in Fig. 2. The TEC map is obtained from the original phase and pseudo-range observations, and the TEC disturbance map comes from the TEC map subtracting the background map, and the ROTI map is grided from the ROTI observations.

TEC map is the most commonly used one among them, and TEC disturbance map is the trend of future development. Belehaki et al. [3] proposed a set of methods for real-time detection and tracking of TID from GNSS observations in Europe, providing more diversified services for European ionospheric monitoring.

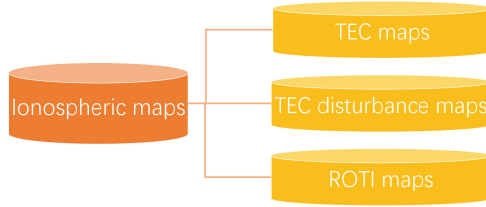


Fig. 2. Outputs of ionospheric real-time monitoring system

### 3 Taking ROTI Map as an Example

#### 3.1 Algorithm for ROTI Map Processing

As one of the products in the ionospheric monitoring system, ROTI map is taken as an example in this section. The data flow from GNSS observation to ROTI map is shown in Fig. 3.

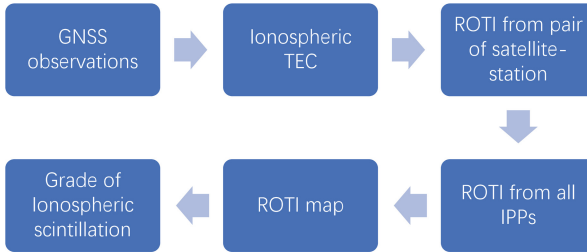


Fig. 3. Data flow of ionospheric ROTI map

The technology of extracting ionospheric TEC from GNSS observation data is very mature. In this paper, the assumption of local spherical symmetry and thin-layer model are adopted, and the vertical TEC estimation is performed station by station, as shown in literature [4]. At first, the ionospheric slant TEC (STEC) should be converted to the vertical TEC (VTEC) at the ionospheric pierce point (IPP):

$$VTEC_{r_m,t_i}^{p_n} = STEC_{r_m,t_i}^{p_n} \times MF(\theta_{r_m,t_i}^{p_n}) \tag{1}$$

Where  $r_m$ ,  $p_n$  and  $t_i$  represents the  $m$ -th GNSS station, the  $n$ -th GNSS satellite and the  $i$ -th epoch.  $\theta$  is the elevation angle at the IPP (generally 350–450 km) towards the satellite. MF stands for mapping function with the expression as follows:

$$MF(\theta_{r_m,t_i}^{p_n}) = \sin \theta_{r_m,t_i}^{p_n} \tag{2}$$

During a continuous period of time, for a pair of one satellite and one monitoring station, the rate of change of VTEC during this period is recorded as ROT (Rate of TEC) in the following formula:

$$ROT_{r_m,t_i}^{p_n} = \frac{VTEC_{r_m,t_i}^{p_n} - VTEC_{r_m,t_{i-1}}^{p_n}}{t_i - t_{i-1}} \tag{3}$$

Correspondingly, the ROTI (Rate of TEC index) can be obtained by statistic of ROT:

$$ROTI_{r_m, t_i}^{p_n} = \sqrt{\left\langle \sum_{j=1}^J (ROTI_{r_m, t_{i-j}}^{p_n})^2 \right\rangle - \left\langle \sum_{j=1}^J ROTI_{r_m, t_{i-j}}^{p_n} \right\rangle^2} \quad (4)$$

Where  $t_{i-j}$  represents the time  $j$  epochs before the current time  $t_i$ ,  $t_{i-1}$  represents the time only one epoch before the current time  $t_i$ .  $J$  is an integer, and  $\langle \rangle$  represents the average.

Now,  $ROTI_{r_m, t_i}^{p_n}$  is a variable closely related to both stations and satellites, referring to the ROTI over a group of discrete IPPs. Since the locations of these IPPs are scattering and may overlap, it is inconvenient to distinguish the ionospheric changes among them. Therefore, a mapping processing is adopted here:

$$GridROTI_{t_i}^{igrd} = \sum_{m=1}^M \sum_{n=1}^N ROTI_{r_m, t_i}^{p_n} / MN \quad (5)$$

Where  $GridROTI_{t_i}^{igrd}$  refers to the ROTI value in the  $igrd$ -th grid at the time  $t_i$ , obtained by averaging the scattering ROTI of all IPPs within the grid at that time. The map is divided by unique step of geographic longitude and latitude, composed of two-dimensional grids.  $M$  and  $N$  denote the number of GNSS stations and visible satellites, respectively.

By Eq. (5), a gridded ROTI map at time  $t_i$  can be obtained. Then, from comparison among the ROTI maps at adjacent moments, the overall trend of ROTI changes is revealed. Furthermore, according to the correlation between ROTI and ionospheric scintillation, the location and amplitude of the ionospheric scintillation can be determined in time.

Considering the ROTI and ionospheric scintillation levelling over the IPPs, the gridded ROTI and ionospheric scintillation is classified into four levels, as shown in the table below. Similar to the algorithm of ROTI map construction, TEC maps are also generated from the IPP VTEC of each pair of station and satellite, without any interpolation method, as gridded map with discrete points to describe the ionospheric TEC (Table 1).

**Table 1.** Relationship of *GridROTI* and ionospheric scintillations classification

Range of <i>GridROTI</i> (unit: TECU/min)	Level of scintillation
[0, 0.1)	None
[0.1, 0.3)	Weak
[0.3, 0.5)	Moderate
$\geq 0.5$	Strong

### 3.2 ROTI Map During a Strong Magnetic Storm

On September 7–8, 2017, the sun erupted with strong coronal mass ejection (CME) events, and the M7.3 and X1.3 class solar flares on 7 September and the M8.1 class

solar flare on 8 September, along with a lot of energy released into interplanetary space. Consequently, the earth's magnetic field undergone two violent disturbance processes and two magnetic storms occurred. The first magnetic storm began approximately at 22:00 UT on September 7, and the second one began near 11:30 UT on September 8. Taking the second magnetic storm as an example, at 13:00 UT on September 8, Dst index reached -120 nT. An hour later, Dst index reached a minimum of -122 nT, and the geomagnetic field recovered to the quiet status until September 11. The geomagnetic Dst indices during this period are shown in Fig. 4. The colors indicate the level of magnetic storm events, green, cyan, orange, and pink color referring to small, moderate, strong, and gigantic geomagnetic storm events, respectively. Seen from Fig. 4, a strong magnetic storm occurred during this period, which means that the energy injected into the earth's magnetic field was very strong, and there are many case studies carried out, such as various changes in the stratosphere and ionosphere.

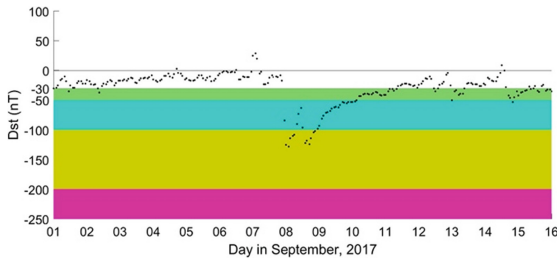


**Fig. 4.** Dst indices in September 1–15, 2017

For example, Dimmock et al. [5] utilized European stations around the polar region to measure the geomagnetically induced current during the magnetic storm, and the results showed that the induced current increased abnormally. Velinov et al. [6] analyzed the number of cosmic ray neutrons during the magnetic storm, and they found that the number of neutrons during the storm decreased sharply and the ionization in the stratosphere was significantly weakened. In addition to the phenomena in the magnetosphere and atmosphere, the response of the ionosphere is also worthy of attention. Yasyukevich et al. [7] analyzed the GNSS TEC from approximately 4,200 global stations during the case of X9.3 class flares on September 6, and found that the global TEC variation differs from the quiet time, 15-16 TECU increase in the low latitude and only 8-10 TECU at the middle latitude. Mendoza et al. [8] used five IGS stations in the Philippines-Taiwan area to analyze the TEC changes in the ionosphere near the equator and confirmed that the TEC increased by about 15 TECU during the storm time.

In particular, for the impact of the magnetic storm on September 8 in and around China, Aa et al. [9] adopted GNSS data from 38 IGS stations in China and 260 station in Crustal Movement Observation Network of China (CMONOC) to extract the TEC map and ROTI map, and found that there is an obvious electron density depletion structure in the ionosphere along the southeast-northwest direction of China, which moved rapidly to high latitudes along the magnetic line. This caused a drastic change in the ionospheric

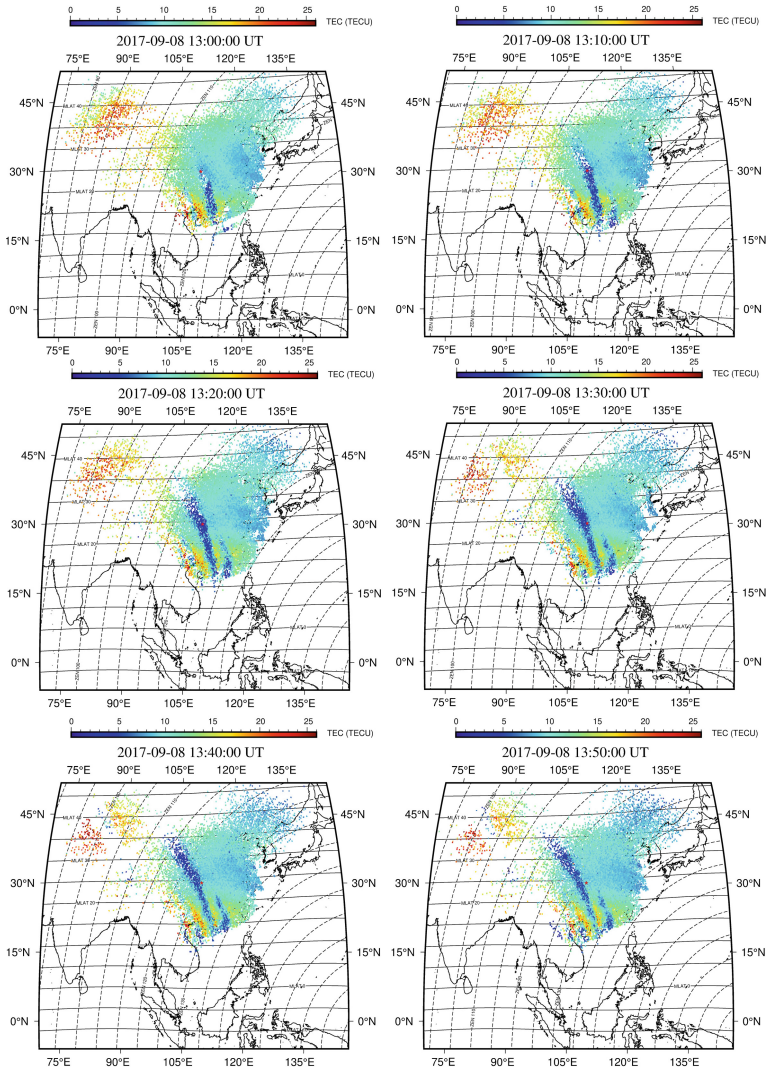


**Fig. 5.** Maps of TEC in and around China during 13:00–14:00 UT on 8 September 2017

TEC, which was reflected in the ROTI map as a strip of ROTI maximum along this direction, and TEC decrease over depletion by about 5–15 TECU.

For comparison, based on the data from 1,292 GNSS stations operated by Qianxun Spatial Intelligence (Zhejiang) Inc., the TEC map and ROTI map during the main phase of the second storm (13:00–14:00 UT, September 8, 2017) are shown in Figs. 5 and 6, respectively, in order to understand the ionospheric response characteristics from a more detailed perspective. In the literature [9], the resolution of the ROTI map is  $1^\circ$  in both the latitude and longitude directions, and the grid ROTI is obtained from the median ROTI value of the IPPs in a grid every 5 min. In this paper, ROTI maps and TEC maps

are obtained under more fine-grained resolution. In detail, the latitude and longitude resolution of the ROTI map is  $0.2^\circ$ , and the time resolution is 30 s. The latitude and longitude resolution of the TEC map is  $0.1^\circ$ , and the time resolution is 15 s.

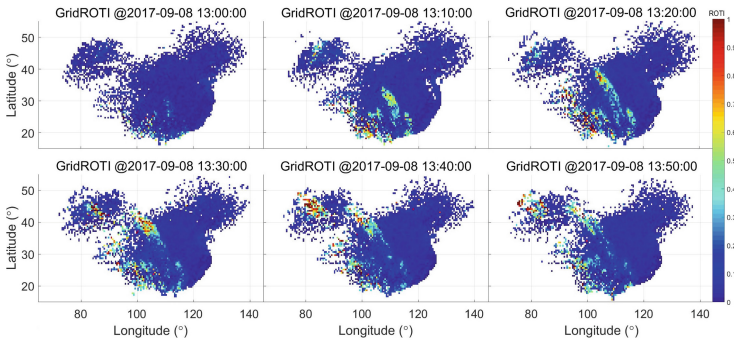


**Fig. 6.** Maps of ROTI in and around China during 13:00–14:00 UT on 8 September 2017

As shown in Fig. 6, the details of the ROTI map are very clear. During the main phase of the magnetic storm, the ROTI in Northeast China and North China was very small, and the time change rate of the ionospheric TEC was very small. Compared with the TEC map in Fig. 5, the ionospheric TEC is mainly controlled by the background and has no obvious fluctuations, which means the GNSS-based positioning in this area is scarcely affected by the magnetic storm. On the contrary, for the link between Gansu and Guangdong, the ionospheric electron density depletion structure generated in low latitudes and quickly propagated along the magnetic line to high latitudes. In Xinjiang, Tibet and other places, due to the lack of observations, only rough changes can be captured. Taking the TEC map around Xinjiang at 13:00 UT as an example, despite the wide blanks, the ionospheric enhancement could be recognized.

Seen from the ionospheric TEC maps in Fig. 5, the ionospheric changes in low-latitude regions such as Guangdong and Guangxi are rather complicated, both the depletion and enhancement in electron density, whose temporal variation indicates that the source of the ionospheric changes comes from the lower latitude regions. As a typical example, Fig. 7 lists the number of GNSS satellites available in Guangdong and Guangxi on September 8, 2017. The standard for “available” satellites is that the time change rate of GNSS TEC is relatively small, with the ROTI from a satellite-station pair is less than a threshold. From 00:00–12:30 UT, the number of available satellites in each constellation system is relatively stable, with the sum above 15. At about 12:30 UT, the number of available satellites turns to drop sharply, even less than 5 satellites available in total, and this worse situation continues until 16:00 UT. It gradually recovers afterwards, returning to a total of more than 15 satellites around 18:00 UT. Particularly, between 12:30–16:00 UT, due to the significant impact upon the ionosphere, the estimation of GNSS TEC will also be affected accordingly. As a result, the ionospheric error in GNSS positioning is difficult to be accurately corrected, which will eventually lead to the increase of positioning error by GNSS. In practice, GNSS positioning requires at least 4 satellites. Notice that, there is a period when the number of available satellites is less than 4, which



means that the positioning cannot be completed only by GNSS observations, and special consideration is needed in applications.

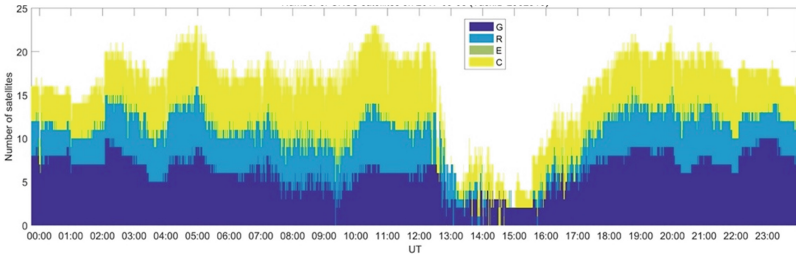


**Fig. 7.** Number of available satellites in Guangdong and Guangxi provinces on 8 Sep., 2017

## 4 Conclusion and Outlook

This paper explains how to utilize the Beidou GBAS in China to develop the framework of the ionospheric real-time monitoring system. As an example, the implementation process of ROTI map is introduced in details. Moreover, both ROTI and TEC maps of China during the main phase of a strong magnetic storm are shown as an example, in order to analyze the different impacts of different regions in China. Guangdong, Guangxi, and Hainan have been significantly affected, where both the electron density depletion and enhancement phenomena coexists. In Gansu and Shanxi provinces, the electron density is mainly depletive, while in Xinjiang and Qinghai, the electron density is mainly enhanced. The entire Northeast and North China are barely affected.

In practice, this real-time ionospheric monitoring system can be landed by getting through the link of the entire architecture, and is still under continuous development so far. In the near future, we look forward to launch it in various applications, as the live weather reports in public lives done.

**Acknowledgements.** This research was supported by the National Natural Science Foundation of China (41704158). The geomagnetic Dst indices comes from the World Data Center for Geomagnetism, Kyoto, Japan.

## References

1. Pi, X., Mannucci, A.J., Lindqwister, U.J., Ho, C.M.: Monitoring of global ionospheric irregularities using the worldwide GPS network. *Geophys. Res. Lett.* **24**(18), 2283–2286 (1997)
2. Cherniak, I., Krankowski, A., Zakharenkova, I.: Observation of the ionospheric irregularities over the Northern Hemisphere: Methodology and service. *Radio Science.* **49**(8), 653–662 (2014)
3. Belehaki, A., Tsagouri, I., Altadill, D., Blanch, E., Borries, C., Buresova, D., Chum, J., Galkin, I., Juan, J.M., Segarra, A., Timoté, C.C.: An overview of methodologies for real-time detection, characterisation and tracking of traveling ionospheric disturbances developed in the TechTIDE project. *J. Space Weather Space Climate* **10**, 42 (2020)

4. She, C., Yue, X., Hu, L., Zhang, F.: Estimation of ionospheric total electron content from a multi-GNSS station in China. *IEEE Trans. Geosci. Remote Sens.* **58**(2), 852–860 (2019)
5. Dimmock, A.P., Rosenqvist, L., Hall, J.O., Viljanen, A., Yordanova, E., Honkonen, I., André, M., Sjöberg, E.C.: The GIC and geomagnetic response over Fennoscandia to the 7–8 September 2017 geomagnetic storm. *Space Weather.* **17**(7), 989–1010 (2019)
6. Velinov, P.I., Tassev, Y.: Long term decrease of stratospheric ionization near the 24-th solar cycle minimum after G4–Severe geomagnetic storm and GLE72 on September 8–10, 2017. *Comptes rendus de l'Académie bulgare des Sciences* **71**(8), 1 Jan 2018
7. Yasyukevich, Y., Astafyeva, E., Padokhin, A., Ivanova, V., Syrovatskii, S., Podlesnyi, A.: The 6 September 2017 X-class solar flares and their impacts on the ionosphere, GNSS, and HF radio wave propagation. *Space Weather* **16**(8), 1013–1027 (2018)
8. Mendoza, M.M., Macalalad, E.P., Juadines, K.E.: Analysis of the Ionospheric Total Electron Content during the Series of September 2017 Solar Flares over the Philippine-Taiwan Region. In: 2019 6th International Conference on Space Science and Communication (IconSpace) 2019 Jul 28, pp. 182–185. IEEE, 28 July 2019
9. Aa, E., Huang, W., Liu, S., Ridley, A., Zou, S., Shi, L., Chen, Y., Shen, H., Yuan, T., Li, J., Wang, T.: Midlatitude plasma bubbles over China and adjacent areas during a magnetic storm on 8 September 2017. *Space Weather* **16**(3), 321–331 (2018)